

Analysis of two stacked cylindrical dielectric resonators in a TE₁₀₂ microwave cavity for magnetic resonance spectroscopy

Saba M. Mattar^{a,*}, Sameh Y. ElNaggar^b

^a Department of Chemistry and Centre for Laser, Atomic and Molecule Sciences, University of New Brunswick, Fredericton, New Brunswick, Canada E3B 6E2

^b Department of Electrical and Computer Engineering, University of New Brunswick, Fredericton, New Brunswick, Canada E3B 6E2

ARTICLE INFO

Article history:

Received 5 November 2010

Revised 7 January 2011

Available online 14 January 2011

Keywords:

Electron paramagnetic resonance

Dielectric resonators

Resonance cavity

Resonator modes

Coupled modes

Resonator frequency

Simulation

Finite element methods

Magnetic field distributions

Filling factor

Resonator conversion factor

Dead time

Resonator bandwidth

Spectrometer sensitivity

Signal-to-noise ratio

ABSTRACT

The frequency, field distributions and filling factors of a DR/TE₁₀₂ probe, consisting of two cylindrical dielectric resonators (DR1 and DR2) in a rectangular TE₁₀₂ cavity, are simulated and analyzed by finite element methods. The TE⁺⁺⁺ mode formed by the in-phase coupling of the TE_{01,δ}(DR1), TE_{01,δ}(DR2) and TE₁₀₂ basic modes, is the most appropriate mode for X-band EPR experiments. The corresponding simulated B⁺⁺⁺ fields of the TE⁺⁺⁺ mode have significant amplitudes at DR1, DR2 and the cavity's iris resulting in efficient coupling between the DR/TE₁₀₂ probe and the microwave bridge. At the experimental configuration, B⁺⁺⁺ in the vicinity of DR2 is much larger than that around DR1 indicating that DR1 mainly acts as a frequency tuner. In contrast to a simple microwave shield, the resonant cavity is an essential component of the probe that affects its frequency. The two dielectric resonators are always coupled and this is enhanced by the cavity. When DR1 and DR2 are close to the cavity walls, the TE⁺⁺⁺ frequency and B⁺⁺⁺ distribution are very similar to that of the empty TE₁₀₂ cavity. When all the experimental details are taken into account, the agreement between the experimental and simulated TE⁺⁺⁺ frequencies is excellent. This confirms that the resonating mode of the spectrometer's DR/TE₁₀₂ probe is the TE⁺⁺⁺ mode. Additional proof is obtained from B_{1,x}, which is the calculated maximum x component of B⁺⁺⁺. It is predominantly due to DR2 and is approximately 4.4G. The B_{1,x} maximum value of the DR/TE₁₀₂ probe is found to be slightly larger than that for a single resonator in a cavity because DR1 further concentrates the cavity's magnetic field along its x axis. Even though DR1 slightly enhances the performance of the DR/TE₁₀₂ probe its main benefit is to act as a frequency tuner. A waveguide iris can be used to over-couple the DR/TE₁₀₂ probe and lower its Q to ≈150. Under these conditions, the probe has a short dead time and a large bandwidth. The DR/TE₁₀₂ probe's calculated conversion factor is approximately three times that of a regular cavity making it a good candidate for pulsed EPR experiments.

© 2011 Elsevier Inc. All rights reserved.

1. Introduction

Pulsed and continuous-wave (CW) electron resonance techniques, such as electron paramagnetic resonance (EPR) [1–6], electron–nuclear double resonance (ENDOR) [4,7–9], electron–electron double resonance (ELDOR) [4,6,10,11], electron spin echo envelope modulation (ESEEM) [9,12,13], double quantum coherence (DQC) [14–16] and double electron–electron resonance (DEER) [12,17–21], are powerful spectroscopic methods for studying the magneto-structural properties of molecules containing unpaired electrons. They are becoming the experimental methods of choice to determine spin–spin distances, geometry, structures and gyromagnetic, fine, and hyperfine tensors of paramagnetic molecules of biological and medicinal significance. The paramagnetic centers in these large biological molecules are usually dilute and the sample size is mostly small and limited. Consequently, consider-

able research is spent on increasing spectrometer sensitivity to facilitate their detection.

One of the ways to increase a spectrometer's sensitivity and signal-to-noise ratio (SNR) is by substituting its resonant cavities by miniature loop-gap (LGR) [22–28] and dielectric (DR) resonators [29–41]. These resonators have several advantages over metal-walled cavities such as small size, low cost, high energy density in the sample vicinity, large magnetic fields (B_1) and filling factors [22–36].

The use of loop-gap resonators is more widespread than DRs and they are now commonly used in EPR spectrometers. They have been reviewed, on more than one occasion, by Hyde et al. [42,43].

As early as 1964 Rosenbaum [29], followed by Walsh and Rupp [37], were the first to employ a DR instead of a cavity in an EPR spectrometer. While DRs have comparable performance to LGRs, some have background signals due to paramagnetic impurities [40]. These may become apparent at low temperatures. Their contribution to the overall spectra is eliminated by subtracting the spectrum of the empty resonator from that containing the sample.

* Corresponding author.

E-mail address: mattar@unb.ca (S.M. Mattar).

The coupling and tuning of a LGR or DR to an EPR spectrometer's microwave bridge is not an easy task [44]. A theoretical account of this subject has recently been given by Mett et al. [45]. For LGRs and DRs coupling is typically carried out by means of a wire loop of appropriate diameter and critical coupling is achieved by varying the distance between the resonator and the loop [22,24,30,35,46]. Waveguide irises [25], Gordon couplers [47] and other antennae [48] have also been used to critically couple LGRs to the spectrometer's microwave bridge.

Usually a shield is used to house LGRs and confine the microwave radiation. Dielectric resonators have been housed in microwave shields as well [32–36]. For example, DRs placed a microwave shield have been used for high pressure [30], stopped flow and rapid scan [33] EPR. The theory of doubly stacked resonators in a microwave shield has been discussed by Jaworski et al. [32].

In addition to the convenient coupling via a waveguide iris, cavities serve the same purpose as a microwave shield and have also been used to house LGRs [49,50] and DRs. A single resonator placed in a TE₁₀₂ cavity was studied by different groups [31,38,40,41]. Nesmalov et al. studied a single ferroelectric resonator in a TM₁₁₀ Cavity [40], while and Golovina et al. employed a cylindrical TE₀₁₁ cavity [38].

The DR/TE₁₀₂ probe used in our laboratory consists of a pair of dielectric resonators, with $\epsilon_r = 29.2$, in an unmodified TE₁₀₂ rectangular cavity. Thus a regular EPR cavity is converted into a dielectric probe with higher SNRs that are at least 24 times larger than the TE₁₀₂ cavity alone [39]. In addition, the frequency of the resonator can be tuned over an extended range. The frequency of the DR/TE₁₀₂ probe is coarsely tuned by varying the distance between the two dielectric resonators. Once the appropriate frequency range is determined, it is then *fine* tuned by keeping that distance constant and changing resonators' positions along the cavity x axis where the sample tube resides. As a result, the two dielectric resonators are asymmetrically positioned in the TE₁₀₂ cavity.

In this article one attempts to numerically assess by simulation [51], using the finite integration methods [52], the microwave electric and magnetic field distributions, sensitivity, filling factors and frequency behavior of the DR/TE₁₀₂ probe used in our EPR spectrometers.

The paper is partitioned as follows. In Section 1 the problem and the goals of the work are presented. Section 2 provides a theoretical background on the linear combination of the electromagnetic fields for two dielectric resonators in a rectangular cavity. In Section 3 a description of the numerical and experimental methods is given while Section 4 is divided into three subsections that present and discuss the results. The first subsection deals with the properties of two identical dielectric resonators symmetrically placed in a TE₁₀₂ cavity while the next section discusses the results of positioning them asymmetrically in the cavity. Section 4.3 compares the magnetic field distributions of one and two resonators in a TE₁₀₂ cavity. Section 5 summarizes the results and conclusions of the work.

2. Theoretical background

In the previous analyses of an EPR probe formed by stacking two dielectric resonators the shield was not considered to be a resonator with distinct resonant modes but simply imposed boundary conditions due to its electrical conducting walls [32,53]. Mett et al. were the first to simulate the effect of a cylindrical cavity as a resonating entity on a single dielectric resonator [54].

In general, two dielectric resonators, DR1 and DR2, in a conducting cavity can be regarded as a combined system of three coupled structures. Consequently, the coupling of any three basic modes

arising from DR1, DR2 and the cavity results in three new modes that are approximated as a linear combination of the basic ones. These new coupled modes will differ from one another according to the relative phases and coupling coefficients of their basic modes. Here, the individual DR1, DR2 and cavity basic modes are TE_{01 δ} , TE_{01 δ} and TE₁₀₂ respectively. They give rise to the three coupled modes, TE⁺⁺⁺, TE⁺⁺⁻ and TE⁺⁻⁻.

Their corresponding spatial electric and magnetic field components, **E** and **B**, are

$$\mathbf{E}^{+++} = a_1^{+++} \mathbf{E}_{01\delta}(\text{DR1}) + a_2^{+++} \mathbf{E}_{01\delta}(\text{DR2}) + a_3^{+++} \mathbf{E}_{102}, \quad (1)$$

$$\mathbf{E}^{++-} = a_1^{++-} \mathbf{E}_{01\delta}(\text{DR1}) + a_2^{++-} \mathbf{E}_{01\delta}(\text{DR2}) - a_3^{++-} \mathbf{E}_{102}, \quad (2)$$

$$\mathbf{E}^{+--} = a_1^{+--} \mathbf{E}_{01\delta}(\text{DR1}) - a_2^{+--} \mathbf{E}_{01\delta}(\text{DR2}) - a_3^{+--} \mathbf{E}_{102}, \quad (3)$$

$$\mathbf{B}^{+++} = b_1^{+++} \mathbf{B}_{01\delta}(\text{DR1}) + b_2^{+++} \mathbf{B}_{01\delta}(\text{DR2}) + b_3^{+++} \mathbf{B}_{102}, \quad (4)$$

$$\mathbf{B}^{++-} = b_1^{++-} \mathbf{B}_{01\delta}(\text{DR1}) + b_2^{++-} \mathbf{B}_{01\delta}(\text{DR2}) - b_3^{++-} \mathbf{B}_{102}, \quad (5)$$

and

$$\mathbf{B}^{+--} = b_1^{+--} \mathbf{B}_{01\delta}(\text{DR1}) - b_2^{+--} \mathbf{B}_{01\delta}(\text{DR2}) - b_3^{+--} \mathbf{B}_{102}. \quad (6)$$

Here a_i^{+++} and b_i^{+++} are the coupling coefficients where the \pm superscripts indicate the relative phase between the modes, which can be either 0° or 180°. The frequency, composition and electromagnetic fields of the new modes will depend on their dimensions and relative positions. As an example, the simulated magnetic field modes, **B**⁺⁺⁺, **B**⁺⁺⁻ and **B**⁺⁻⁻, are schematically drawn in Fig. 1a–c.

The comparison of Fig. 1a–c shows that the modes in Fig. 1a and b have a larger TE₁₀₂ component than that in Fig. 1c. The small TE₁₀₂ component of TE⁺⁻⁻, causes its **B**⁺⁻⁻ fields, shown in Fig. 1c, to be very small near the cavity walls. Therefore this mode is not suitable for the exciting the DR1 and DR2 resonators via the cavity iris.

The further comparison of Fig. 1a and b in the vicinity of DR1 and DR2 shows that **B**⁺⁺⁺ is larger than **B**⁺⁺⁻.

Consequently, using the TE⁺⁺⁺ mode should result in a spectrometer with a relatively higher SNR and sensitivity.

In general, linear combinations of other TE _{mnp} , TM _{mnp} and hybrid modes may also exist. For example the DR1 and DR2 TE_{01 δ} modes may form linear combinations with the cavity's TE₁₀₁ mode, as will be shown later.

3. Computational and experimental details

A computer employing two Quad-Core Opteron 2350 Processors, with 3 GB of RAM and running Windows XP was used for the simulations. The DR/TE₁₀₂ properties were calculated using the Computer Simulation Technology (CST), suite of programs [51]. The dimensions, relative positions in space and dielectric constants of DR1, DR2 and cavity are used as inputs. The program solves Maxwell's equations, using an eigenvalue formalism, from which the frequencies, filling factors, electric and magnetic field distributions are calculated. The program can use two methods for solving the eigenvalue problem. The first is the Jacobi–Davidson (JD) method [55], while the second is the Advanced Krylov Subspace (AKS) method [56]. The JD method is computationally expensive and time consuming but is robust when solving degenerate modes. Since, due to its low symmetry, the system under consideration has no degeneracies, the faster AKS method was used. During the solution, the system's geometry is spatially partitioned into a mesh of grid elements. The equations are then solved using these grid elements by the finite integration technique (FIT) [52].

The EPR spectrum of the Mn²⁺/CaO sample, used as a reference standard, was recorded with a modified Varian E104 spectrometer [39]. The frequency of the DR/TE₁₀₂ resonator was measured with a Hewlett-Packard model HP5340A frequency counter and the

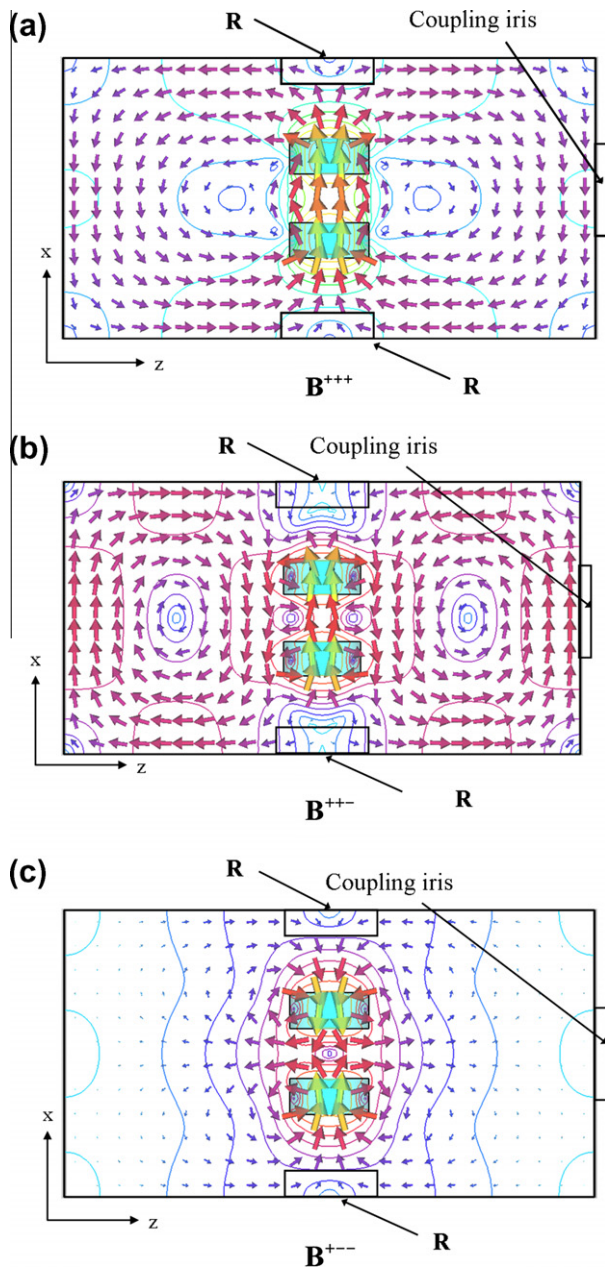


Fig. 1. Simulated resonant magnetic field modes of two identical dielectric resonators in a cavity. (a) Magnetic field, \mathbf{B}^{+++} where all three basic modes are in-phase. The individual characteristics of the basic $TE_{01\delta}$ and TE_{102} modes are evident. Also shown are the regions of the coupling iris and chimneys (R) where the sample enters the cavity. (b) Both resonators are out of phase with the cavity. (c) Only one resonator is in-phase with the cavity. DR1 and DR2 are out of phase.

microwave power was measured with an HP432C digital power meter equipped with an HP478A thermistor power head. The meter's output was digitized via a National Instruments ATMIO16E10 data acquisition board. No signals due to paramagnetic impurities from DR1 and DR2 were apparent.

4. Results and discussion

4.1. Resonators symmetrically placed within a cavity

In our previous work, the frequency of the DR/ TE_{102} probe was coarsely adjusted by changing the distance between DR1 and DR2. In this way, the frequency of the DR/ TE_{102} probe could be varied by

approximately 2.0 GHz [39]. However it was not known if the frequencies spanning that range were due to one or more resonant modes. To resolve this point, two dielectric resonators placed in a cavity are modeled using the CST program. The dimensions of the resonators correspond to those obtained from Murata (Model DRT060R020C0227B, $\epsilon_r = 29.2$). The cavity dimensions were taken from the X-band E-231 Varian TE_{102} cavity. The cylindrical axes of DR1 and DR2 were aligned with the cavity's x-direction, as shown in the Fig. 2.

The frequencies of the simulated lowest five modes are shown in Fig. 3. They were calculated as d_{12} was increased by symmetrically shifting DR1 and DR2 from the center of the cavity. The inspection of the magnetic field distribution of these modes indicates that the lowest mode, TE' , is a result of the in-phase interaction of the $TE_{01\delta}$ modes of the dielectric resonators and the TE_{101} mode of the cavity. Its magnetic field takes the form

$$\mathbf{B}' = c_1^{+-+} \mathbf{B}_{01\delta}(\text{DR1}) - c_2^{+--} \mathbf{B}_{01\delta}(\text{DR2}) - c_3^{+++} \mathbf{B}_{101}. \quad (7)$$

The frequency of the TE' mode changes from 6.55 to 7.25 GHz as d_{12} spans the range of 17 mm. It is out of the range of interest (8–10 GHz) and will not be considered further.

At any given distance the TE^{+++} frequency is always the lowest of the three remaining TE^{+++} , TE^{+-+} and TE^{+--} modes. One of the reasons for coarse tuning the DR/ TE_{102} probe by changing the distance between DR1 and DR2 was the linear response of the frequency with d_{12} [39]. The TE^{+++} in Fig. 3 also displays this desirable feature and changes almost linearly by 850 MHz as d_{12} is varied from 1 to 17 mm. Therefore the lower end of the frequency range obtained experimentally by coarse tuning most probably corresponds to the lowest TE^{+++} mode. In contrast, Fig. 3 indicates that the frequency change of the TE^{+-+} and TE^{+--} modes is complicated and nonlinear.

When comparing previous results, it is important to differentiate between a stacked resonator pair in a cavity and those placed in a shield. If the small cylindrical "tight" shield has a radius comparable to those of DR1 and DR2 [32,35], then it acts only as a microwave shield with very little interaction with the dielectrics. However in the case of a cavity whose internal dimensions exceed $\lambda/4$ and its frequency is comparable to that of the two combined resonators, then significant interactions will occur between DR1, DR2 and the cavity. A similar reasoning was proposed by Mett et al. in the case of one dielectric resonator in a cavity. They found that the interaction was maximum when the frequencies of the dielectric resonator and the cavity were the same [54]. If the shield is considered to be a cylindrical cavity, the frequency of its TE_{011} mode can be calculated using

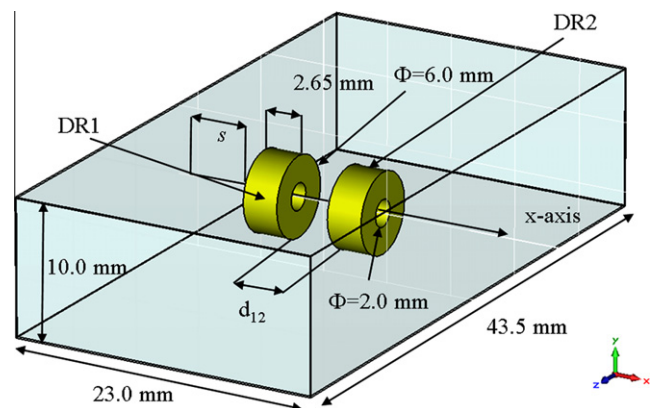


Fig. 2. Two identical dielectric resonators, DR1 and DR2 in a TE_{102} cavity. The distance between DR1 and DR2 is d_{12} and the distance of DR1 from the cavity wall is s . The dimensions of the two resonators and the cavity are also shown.

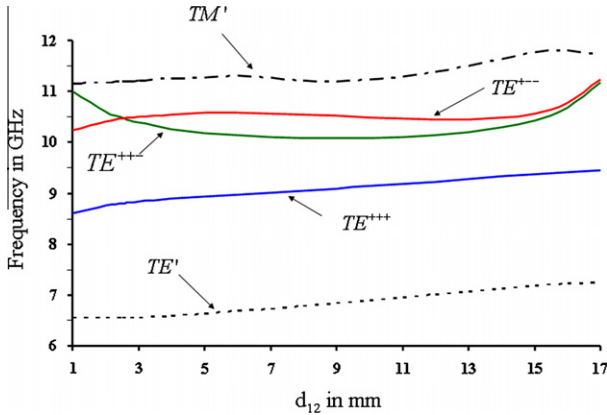


Fig. 3. Frequencies of the TE' , TE^{+++} , TE^{+-+} , TE^{+--} and TM' modes as a function of the separation between the dielectric resonators, d_{12} .

$$f_c = \frac{c}{2\sqrt{\epsilon_r}} \sqrt{\left(\frac{x'_{01}}{\pi r_c}\right)^2 + \left(\frac{1}{\ell_c}\right)^2}. \quad (8)$$

Here x'_{01} is the first root of $J'_0(x)$ Bessel function [54], r_c the radius and ℓ_c the length of the cylindrical shield. If the shield is entirely filled with Delrin[®] ($\epsilon_r = 2.53$) and has the dimensions given by Sienkiewicz et al. [35] its frequency is approximately 19.8 GHz. On the other hand if the shield is empty ($\epsilon_r = 1.0$) its frequency jumps to 31.4 GHz. Therefore in the case where the shield is partially filled with Delrin[®], [32,35] its actual frequency is expected to lie between these two frequencies. Any frequency in that range would be too high for the shield to significantly interact with DR1 and DR2. Thus the TE^{+++} mode has no counterpart in the case of doubly stacked dielectric resonators in a tight shield [32].

To better understand the differences between the frequencies and modes of two DRs in a cavity and a tight shield, the frequency of the *symmetric mode* resulting from the coupling of two dielectric resonators in free space was calculated [53]. The calculated frequencies were compared to experimental measurements in Table 2 of Jaworski et al. [32]. The results gave an excellent correlation provided that the calculated values were scaled up by a factor of 1.09. This is within the known 10% accuracy of the magnetic wall model used [57]. These results corroborate that the lowest resonant mode of two dielectric resonators in a tight shield are indeed due to the symmetric mode of the doubly stacked resonators [32]. It also indicates that both methods of frequency calculation yield comparable results [32,53].

In summary, the TE^{+++} mode is due to the resonant interaction of the in-phase interaction of the DR1, DR2 and the rectangular TE_{102} cavity. On the other hand, the mode observed by Jaworski et al. [32] is due to the in-phase interaction of the two dielectrics with insignificant interactions with the cylindrical shield.

Fig. 3 indicates that as d_{12} gets larger DR1 and DR2 approach the cavity walls and the TE^{+++} frequency approaches the resonant frequency of an empty TE_{102} cavity. The regions shown as rectangles, R, in Fig. 1 have very small magnetic fields, \mathbf{B}_{102} . This leaves the contributions from $\mathbf{B}_{01\delta}(\text{DR1})$ and $\mathbf{B}_{01\delta}(\text{DR2})$.

These are also negligible in the R regions due to the following reasons. The surfaces of DR1 and DR2 may be approximated as magnetic walls due to the large difference between their $\epsilon_r = 29.2$ and that of the cavity interior ($\epsilon_r = 1$). Hence, the tangential components of $\mathbf{B}_{01\delta}(\text{DR1})$ and $\mathbf{B}_{01\delta}(\text{DR2})$ in the yz planes are approximately zero. Assuming that the cavity has perfectly conducting walls, then the normal component of \mathbf{B}^{+++} vanishes at its surface. To maintain the continuity of \mathbf{B}^{+++} in space then the normal components of $\mathbf{B}_{01\delta}(\text{DR1})$ and $\mathbf{B}_{01\delta}(\text{DR2})$ facing the cavity walls in the R regions must also be very small. Only minor perturbations due to

$\mathbf{B}_{01\delta}(\text{DR1})$ and $\mathbf{B}_{01\delta}(\text{DR2})$ in the parts that face the interior of the cavity will exist. The net result is that in these two R regions $\mathbf{B}^{+++} \approx 0$. Consequently when the two DRs are very far apart, the overall \mathbf{B}^{+++} distribution in the entire DR/ TE_{102} probe is approximately equal to that of an empty TE_{102} cavity. The same reasoning also applies to \mathbf{E}^{+++} and as a result, the frequency of the DR/ TE_{102} probe will also be close to that of a rectangular TE_{102} cavity.

Jaworski et al. have also determined that, in the case of two resonators placed in a tight shield, the nearest spurious mode to the EPR active mode is approximately 400 MHz higher and is TM in character. They also found that this frequency difference is almost constant over the entire range studied (0 to 4.5 mm) [32]. In the present case of DR1, DR2 in a cavity, the first TM mode encountered is labeled as TM' and shown in Fig. 3. Its frequency also increases almost linearly and is approximately 2.1–2.5 GHz higher in frequency than the TE^{+++} mode. This relatively large frequency gap is attributed to the additional interaction of the DR1, DR2 with the cavity as compared to the tight microwave shield.

The magnitude of \mathbf{B}^{+++} in the vicinity of the sample is an important parameter since it directly affects the filling factor, sensitivity and the SNR of the spectrometer [22,32,54]. For an allowed transition, where $\Delta M_S = \pm 1$, the effective component of \mathbf{B}^{+++} must be perpendicular to the external homogenous static magnetic field, \mathbf{B}_0 . Consequently, the x component of \mathbf{B}^{+++} (hereafter referred to as B_{1x}) was calculated along the cavity x axis, where the sample resides, as a function of d_{12} . Again, d_{12} was increased by symmetrically shifting DR1 and DR2 from the center of the cavity. Fig. 4a shows the results of these calculations where the two B_{1x} maxima, corresponding to the positions of DR1 and DR2, move away as the d_{12} increases. However between the two maxima is a valley that is always nonzero. This implies that in the DR/ TE_{102} probe, the DR1 and DR2 are never fully decoupled. According to Eq. (4), B_{1x} is due to the two dielectric resonators and the cavity. To separate the contributions from the three components, the calculated B_{1x} for the empty cavity was also drawn in Fig. 4a. From this figure, it is obvious that for $d_{12} = 16.0$ mm, where DR1 and DR2 are farthest from one another, the calculated B_{1x} is predominantly due to the cavity around its center (7–15 mm) as indicated by the vertical dashed lines.

To further emphasize this point, the difference between the B_{1x} fields of the DR/ TE_{102} probe and the empty cavity were plotted in Fig. 4b. It shows that when $d_{12} = 16.0$ mm and the two resonators are far apart B_{1x} is very close to zero in the center of the cavity. The minute positive values around $x = 11$ – 12 mm are due to the dielectric resonators' tails, which fall off exponentially with distance. Thus, one may conclude that even at $d_{12} = 16.0$ mm there is still some small coupling between the two resonators and is accentuated by the presence of the cavity.

It is worth noting from Fig. 4a that the values of the B_{1x} maxima when $d_{12} = 2.0$ mm is around 4.0 Gauss (G) while at $d_{12} = 8.0$ mm it is approximately 3.4 G. Therefore one estimates that at $d_{12} = 4.0$ mm it is ~ 3.7 G. This is comparable to the B_{1x} of commercial resonators, such as the Bruker[®] ER4118X-MD5 dielectric Flexline probe. It is also comparable to our previous experimental calculations of B_{1x} which is 4.4 G [39]. However, one must note that in our experimental setup the two dielectric resonators were not symmetrically placed in the TE_{102} cavity [39]. As will be shown later, this has the effect of further increasing the magnitude of the B_{1x} maximum.

4.2. Resonators asymmetrically placed within the cavity

As mentioned previously, the main aim of this paper is to understand theoretically and analyze numerically the design, microwave characteristics and sensitivity of the DR/ TE_{102} probe [39]. The frequency of the probe was *fine* tuned by keeping the

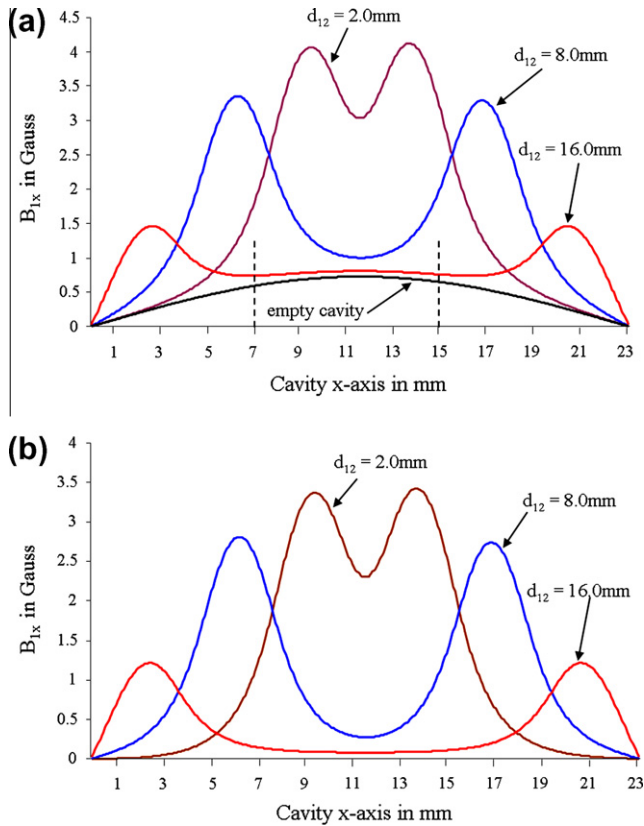


Fig. 4. (a). Magnetic field, B_{1x} , calculated along the cavity x axis at selected d_{12} distances. Also included is B_{1x} due to the empty TE_{102} cavity. (b) Magnetic field, B_{1x} , after subtraction of the empty cavity contribution.

d_{12} distance constant and varying the distance along the cavity x axis, s , shown in Fig. 2. This causes the DR1 and DR2 to be inequivalent and asymmetrically positioned in the cavity. To simulate the fine tuning process, d_{12} was fixed at 4.0 mm and the two resonators were moved along the cavity x axis by varying s from 0.5 mm to 6.85 mm. At the end of the range when $s = 6.85$ mm, DR1 and DR2 are symmetric and equivalent.

The frequency of the TE^{+++} mode, calculated by the CST program, as a function of s is depicted in Fig. 5. It shows that as s is varied by 6.35 mm, the corresponding frequency change is almost 213 MHz. This is approximately one quarter of the frequency range spanned in Fig. 3 as a result of changing d_{12} from 1.0 mm to 17 mm.

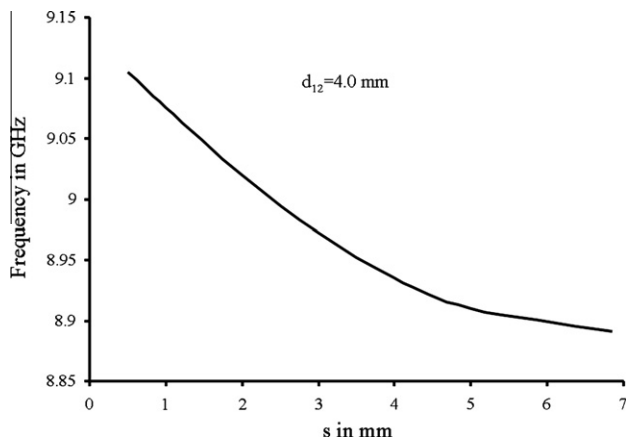


Fig. 5. Frequency change as a function of the distance, s , for the asymmetric TE^{+++} mode.

The frequency change per mm in the former case is 50 MHz/mm while that of the latter is 33.5 MHz/mm. Although these tuning rates are comparable, it is easier to fine tune the resonator by moving DR1 and DR2 in tandem.

The simulated \mathbf{B}^{+++} fields of this mode are depicted in Fig. 6. The comparison of \mathbf{B}^{+++} in this figure and Fig. 1a indicates that the asymmetric TE^{+++} mode still has a considerable TE_{102} component. In addition the \mathbf{B}^{+++} vectors have significant amplitudes at the cavity's iris, DR1 and DR2. Therefore efficient coupling between the microwave bridge and the dielectric resonators is achieved. The figure also indicates that magnetic field density in the vicinity of DR2 is higher than that near DR1.

The same boundary condition arguments put forward for the symmetric case when both resonators were close to the cavity walls in the R regions also apply in the asymmetric case for DR1 only. Thus in this case DR1 only acts as a tuner with little influence on \mathbf{B}^{+++} and \mathbf{E}^{+++} .

When $d_{12} = 4.0$ mm and $s = 0.5$ mm, which corresponds to the original experimental setup, the calculated frequency of the TE^{+++} mode is very close to the experimental frequency [39]. Therefore, it is highly likely that the experimental operating mode of the DR/ TE_{102} probe is actually the TE^{+++} mode.

To prove that the asymmetric TE^{+++} mode is the experimental mode in question, a series of additional experiments were performed. The exact experimental conditions were simulated. This involved including a Teflon holder for DR1 and DR2. In addition, a quartz tube with an inner diameter of 0.6 mm was used as a sample holder. Finally, CaO with a very small amount of Mn^{2+} , as a substitutional impurity, was also included. The complete structure, its dimensions and relative dielectric constants of the materials used in the calculations are shown in Fig. 7 and Table 1. The top of DR2 was maintained at the center of the cavity and DR1 was allowed to move along the cavity x axis. The distance from the bottom of the cavity to the bottom of DR1, s , was varied from 2.0 mm to the limit of 5.0 mm. In this limit DR1 and DR2 almost touch one another.

As s was varied, the spectrometer's frequencies were measured and compared to those calculated, by the CST program.

Fig. 8 shows that the agreement between the experimental and computed values is excellent. The maximum deviation between them is approximately 0.22%. Since by taking into consideration all the experimental details the simulator reproduces the experimental frequencies, then this indicates that the method is accurate and reliable. It also proves that the resonating mode used in the spectrometer is indeed the TE^{+++} mode. This gives us confidence to use these types of simulations to design and verify similar dielectric resonator probes and understand how some of the

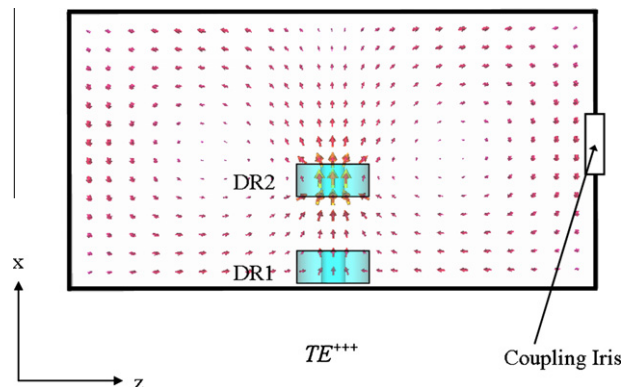


Fig. 6. Simulated \mathbf{B}^{+++} mode at $d_{12} = 4.0$ mm and $s = 0.5$ mm showing the in-phase relation between the three basic modes. Note the larger \mathbf{B}^{+++} values within the central resonator, DR2.

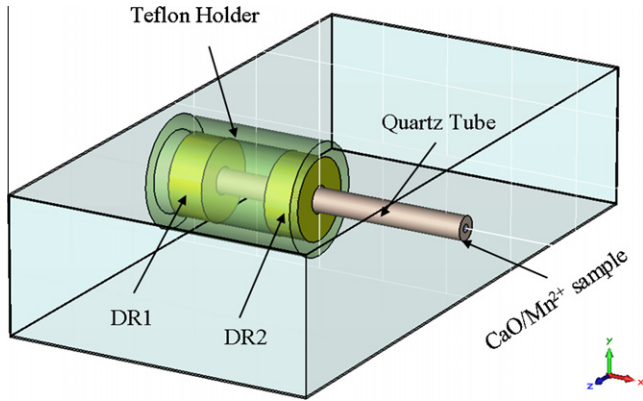


Fig. 7. Schematic diagram of the DR/TE₁₀₂ probe used in the recording the CaO/Mn²⁺ spectra.

Table 1
Dimensions and relative dielectric constants of materials used in the simulations.

Material	ID (mm)	OD (mm)	Relative dielectric constant, ϵ_r
Cavity			1.0
DR1, DR2	2.0	6.0	29.2
Teflon	6.0	8.2	2.1
Quartz	0.6	1.8	3.75
CaO/Mn ²⁺	0.6	0.6	11.8

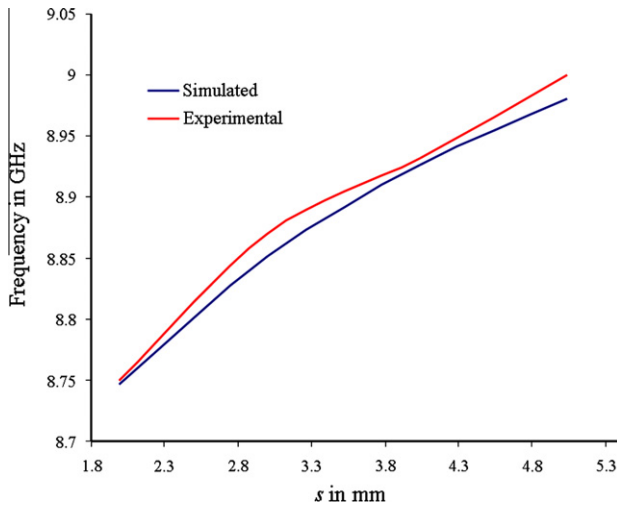


Fig. 8. Frequency change as a function of the distance, s , for the calculated and experimental asymmetric TE⁺⁺⁺ mode.

existing ones function. Further confidence in the method arises from the calculation of B_{1x} and filling factors discussed below.

One is now in a position to investigate the behavior of B_{1x} when DR1 and DR2 are moved in space to go from the symmetric configuration to the experimental asymmetric one. The B_{1x} fields for the experimental configuration can also be calculated as was done previously for the symmetric case. In this case d_{12} was fixed at 4.0 mm and both resonators were moved as a single unit along the cavity x axis. Thus s was changed from 0.1 to 6.85 mm. Seven selected s values were chosen and the simulations repeated. For clarity these results are broken up into two Fig. 9a and b.

Fig. 9a shows that when $s = 6.85$ mm, which corresponds to the symmetric positioning of DR1 and DR2, the maximum of $B_{1x} \approx 3.77$ G. This value is very close to the interpolated value predicted in the previous section. When s is decreased, DR1 and DR2 move

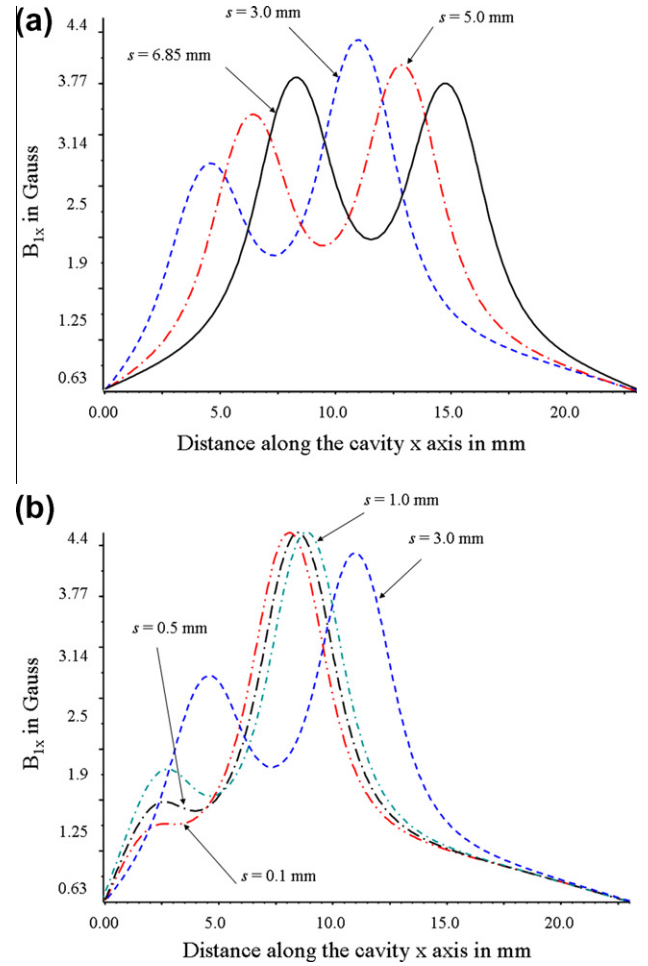


Fig. 9. (a) Magnetic field B_{1x} for $s = 6.85, 5.0$ and 3.0 mm. (b) B_{1x} for $s = 3.0, 1.0, 0.5$ and 0.1 mm.

towards the bottom wall; become asymmetrically positioned within the cavity and the two maxima of B_{1x} around DR1 and DR2 become different. While B_{1x} of DR1 decreases that of DR2 increases. Fig. 9b indicates that at the extreme position when $s = 0.1$ mm and DR1 is very close to the cavity wall, its B_{1x} maximum is a shoulder that is barely resolved under that of the DR2 wing.

It is important to note from Fig. 9b, that at the experimental configuration ($s = 0.5$ mm) B_{1x} maximum at DR2 is calculated to be ≈ 4.4 G. This is almost identical to the experimental B_{1x} value measured previously [39]. This is further proof of the accuracy of the simulations and that the resonating mode of the DR/TE₁₀₂ probe is the TE⁺⁺⁺ mode. Consequently to get the maximum spectral intensity and filling factors, a small sample should be placed in the DR2 resonator and fill its inner hole.

The next step is to calculate the asymmetric filling factor. It is defined as [32,58]

$$\eta = \frac{\int_{V_{\text{Sample}}} |H_{1x}|^2 dv}{\int_{V_{\text{cavity}}} |\mathbf{H}_1|^2 dv} \equiv \frac{\int_{V_{\text{Sample}}} |B_{1x}|^2 dv}{\int_{V_{\text{cavity}}} |\mathbf{B}_1|^2 dv}, \quad (9)$$

where

$$B_{1x} = \mu_0 H_{1x}, \quad (10)$$

and μ_0 is magnetic permeability in free space. However the time averaged magnetic energy stored in the entire DR/TE₁₀₂ probe volume, V_{cavity} , is [59]

$$W_M = \frac{1}{4\mu_0} \int_{V_{cavity}} |B_1|^2 dv. \tag{11}$$

Therefore

$$\eta = \frac{\int_{V_{sample}} |B_{1x}|^2 dv}{4\mu_0 W_M}. \tag{12}$$

The CST program normalizes, the total energy to 1.0 J. Thus Eq. (12) becomes

$$\eta \approx \frac{1}{2\mu_0} \int_{V_{sample}} |B_{1x}|^2 dv, \tag{13}$$

or

$$\eta \approx \frac{\pi r^2}{2\mu_0} \int_0^\ell |B_{1x}|^2 dx. \tag{14}$$

Here ℓ is the length of the sample and r is the radius of the DR2 inner hole. It is equal to 1.0 mm. In the case of a sample inside the hole of DR2, hereafter referred to as the “small sample”, with $s = 6.85$ mm the calculated η is relatively small. As s decreases, η increases and starts to saturate at $s = 0.8$ mm, as shown in Fig. 10. The relatively large filling factor at the experimental setting, corresponding to $s = 0.5$ mm in Fig. 10, results in the largest SNR because it is directly proportional to η ,

$$SNR \propto \eta Q \sqrt{P}. \tag{15}$$

The η values when the sample fills the entire tube are also calculated and drawn in Fig. 11. In this case, the integral limits in Eq. (14) span the whole cavity x axis in contrast to the small sample in Fig. 10 where one only integrates over the height of DR2. Thus it is not surprising that the comparison of Figs. 10 and 11 indicates that η is smaller for the small sample. This simply implies that the larger sample results in a stronger signal albeit inhomogeneous.

One should warn that for large aqueous samples dissipative losses will decrease the sensitivity by degrading the quality factor.

Fig. 11 also indicates that η increases as s increases and eventually saturates at $s = 6.85$ mm. According to Eq. (14) η is proportional to the area under the curve in Fig. 12. It shows that the area under the curve for $s = 0.1$ mm is slightly less than that for $s = 6.85$ mm and explains the $\sim 21\%$ increase in η as s increases in Fig. 11. Beyond $s = 6.85$ mm the curve becomes its mirror image. As s increases further the DR2 resonator face ultimately reaches a distance of 0.5 mm from the opposite wall. This is the mirror image of the original experimental setting.

One may estimate the EPR signal enhancement (SE) due to the different filling factors of the DR/TE₁₀₂ probe and the TE₁₀₂ empty cavity and compare it with our previous experimental results [39]. According to Nesmelov et al. [40], if one assumes that the quality

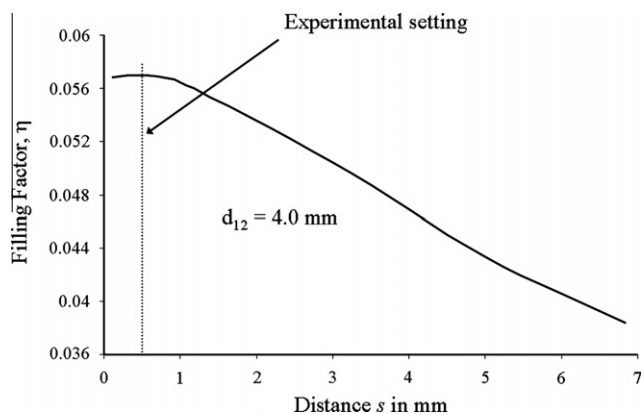


Fig. 10. Filling factor of the small sample as a function of the distance s .

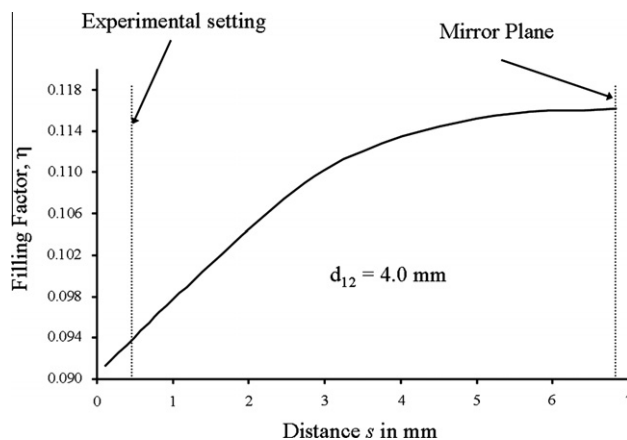


Fig. 11. Filling factor of a long sample tube as a function of the distance s .

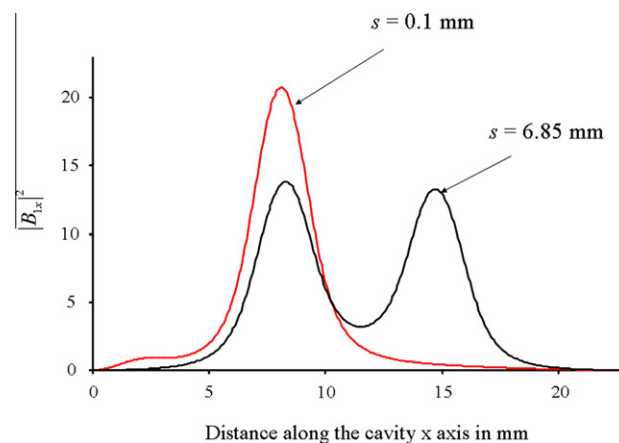


Fig. 12. Plot of $|B_{1x}|^2$ as a function of the cavity x axis for $s = 0.1$ and 6.85 mm.

factor does not change appreciably by the insertion of DR1 and DR2, then the SE (ratio of signal intensities $S_{DR/TE_{102}}$ and $S_{TE_{102}}$) is related to their corresponding filling factors, $\eta_{DR/TE_{102}}$ and $\eta_{TE_{102}}$, by

$$SE = \frac{S_{DR/TE_{102}}}{S_{TE_{102}}} \propto \frac{\eta_{DR/TE_{102}}}{\eta_{TE_{102}}}. \tag{16}$$

In reality the EPR signal intensity depends on many parameters besides the filling factor such as temperature, relaxations times, nature of the host lattice, concentration of the paramagnetic species and the degree of its saturation. Consequently, in our previous work [39] the SE of the various samples tested varied from 24 to 35. The calculated SE in this study is approximately 32.5 which is in good agreement with those determined experimentally [39].

4.3. Comparison with a single resonator in a TE₁₀₂ cavity

The DR/TE₁₀₂ probe is compared to the case when only one resonator is in the cavity. To make the comparison meaningful the single resonator was placed in the exact same position of DR2 of the DR/TE₁₀₂ probe. This was followed by simulating and plotting its B_{1x} in Fig. 13. It shows that the B_{1x} maximum value due to DR1 and DR2 is slightly larger than the corresponding one for a single resonator. This is because the high dielectric constant of the second resonator (DR1) collimates the magnetic field of the TE₁₀₂ cavity mode along its x axis. This also explains why the calculated filling factor for the doubly stacked resonator at the experimental position ($s = 0.5$ mm, $\eta = 0.057$) is slightly higher than that for a

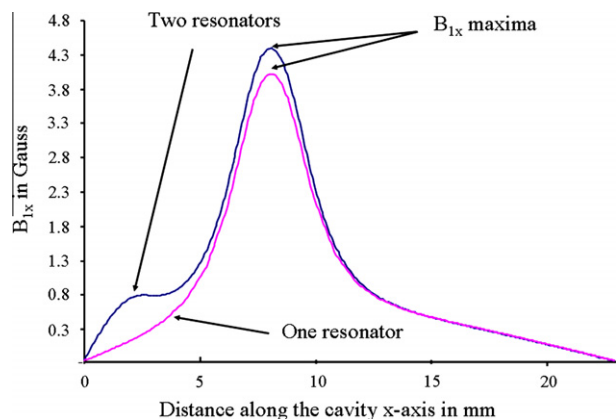


Fig. 13. Comparison of B_{1x} for one and two dielectric resonators in a cavity.

single resonator calculated to be 0.048. Therefore although the two curves are different, their B_{1x} maxima, shown in Fig. 13, are close to one another and DR1 mainly acts as a frequency tuner.

Since the second resonator mainly functions as a tuner, it is not necessary to have a hole in it. Recalculating the frequency with DR1 as a solid cylindrical pill caused the probe frequency to decrease by approximately 60 MHz.

From the above arguments, Figs. 6 and 13, one may conclude that the DR/TE₁₀₂ probe is very similar to a single resonator in a cavity. This is in agreement with the experimental results of Nesmelov et al. [40] where the DR simply redistributes the microwave fields within the cavity, and focuses B_{1x} inside its hole leading to an increase in η .

Finally a rough estimate of the DR/TE₁₀₂ conversion factor, C_p , is made. According to Blank et al. [41]

$$C_p = \frac{B_1}{\sqrt{P}}, \quad (17)$$

where P is the incident power. From this C_p is estimated to be $\approx 4.4 \text{ G}/\sqrt{\text{W}}$. It is in the same range of loop-gap resonators [24] and other commercial probes, such as the Bruker® ESP380-1052-DLQ-R/N/H. On the other hand, C_p for a rectangular TE₁₀₂ cavity alone ranges from 1.1 to 1.4 $\text{G}/\sqrt{\text{W}}$ [40,41,48]. Thus the DR/TE₁₀₂ probe has a C_p that is approximately three times that of a regular cavity and makes it a viable resonator for a pulsed EPR spectrometer. In addition, the simplicity of over-coupling the DR/TE₁₀₂ probe, using its regular cavity iris [39], allows one to easily lower its Q to ≈ 150 . Under these conditions, it has a large bandwidth and a relatively short dead time. It is currently being tested in our laboratory for use in pulsed EPR experiments.

5. Summary and conclusions

The frequency, filling factors and field distributions of the DR/TE₁₀₂ probe, made up of two dielectric resonators in a rectangular cavity, are assessed by simulation using the finite integration technique.

The TE⁺⁺⁺ mode of the DR/TE₁₀₂ probe, formed by the in-phase coupling of the TE_{01δ}, TE_{01δ} and TE₁₀₂ basic modes, is found to be the most suitable mode for X-band EPR experiments. It resonates in the right frequency range and can be conveniently coarse tuned because its frequency changes almost linearly by 850 MHz as the distance between DR1 and DR2, d_{12} , changes from 1 to 17 mm. It can be further fine tuned by moving DR1 and DR2 in tandem along the cavity x axis. The frequency change per mm in the coarse tuning process is 50 MHz/mm while for fine tuning it is 33.5 MHz/mm. However, it is more convenient to fine tune the DR/TE₁₀₂ probe frequency by changing s asymmetrically instead of changing d_{12} .

For the probe to be efficient, its \mathbf{B} fields should be significantly large at DR1, DR2 and the cavity's coupling iris. The simulated \mathbf{B}^{+++} fields of the fine-tuned asymmetric TE⁺⁺⁺ mode fulfill this condition. Therefore efficient coupling between the microwave bridge and the dielectric resonators is still maintained. It is also found that \mathbf{B}^{+++} in the vicinity of DR2 is larger than that near DR1 indicating that DR1 merely acts as a tuner with little influence on \mathbf{B}^{+++} .

In addition to DR1 and DR2, the cavity is found to be an essential component of the probe and plays an important role in affecting its frequency and properties. For example when d_{12} is large and the dielectric resonators are close to the cavity walls, the TE⁺⁺⁺ frequency and \mathbf{B}^{+++} distribution are very close to that of an empty TE₁₀₂ cavity. The plot of B_{1x} versus d_{12} along the cavity x axis shows that DR1 and DR2 are never fully decoupled. Even at $d_{12} = 16.0$ mm some coupling still exists and is accentuated by the presence of the cavity.

On the other hand, for a tight shield the EPR active mode is only due to the in-phase interaction of DR1 and DR2 with insignificant interactions with the shield. There is no counterpart for the TE⁺⁺⁺ mode of the DR/TE₁₀₂ probe in this case. In addition, the frequency of the nearest spurious TM mode in the case of a tight shield is approximately 400 MHz higher than the EPR active mode. However, for a DR1, DR2 and a cavity, the first TM mode is approximately 2.1–2.5 GHz higher in frequency than the TE⁺⁺⁺ mode. This larger frequency gap is ascribed to the additional interaction of the cavity with DR1 and DR2 in comparison to the tight microwave shield.

If all the experimental details are taken into consideration, the agreement between the experimental and simulated TE⁺⁺⁺ frequencies confirms that the resonating mode of the DR/TE₁₀₂ probe used in the spectrometer is the TE⁺⁺⁺ mode.

At the experimental configuration DR1 is very close to the cavity wall and its B_{1x} is small compared to that of DR2. The calculated B_{1x} maximum due to DR2 is 4.4 G and is almost identical to the measured experimental value. This is additional proof that the DR/TE₁₀₂ mode is TE⁺⁺⁺ and that the simulations are accurate.

The filling factors, η , for a small sample and when the sample fills the entire tube are calculated. For the experimental configuration, the small sample $\eta = 0.057$ while for the entire sample tube it is larger (0.094) and indicates that a larger sample gives a stronger signal. However the B_{1x} across the sample length is not homogenous.

When the B_{1x} of the DR/TE₁₀₂ probe is compared to that of only one resonator in the cavity, its B_{1x} maximum value is found to be slightly larger than that for a single resonator. This is because the second resonator (DR1) further concentrates the cavity \mathbf{B}_{102} along its x axis. Accordingly the filling factor, η , for the doubly stacked resonator is 0.057 and is somewhat higher than 0.048 for a single resonator. Although DR1 only slightly increases the performance of the DR/TE₁₀₂ probe its main advantage, as mentioned previously, is to act as a frequency tuner.

The DR/TE₁₀₂ probe has a C_p that is approximately three times that of a regular cavity and can be easily over-coupled, using its regular waveguide iris, to lower its Q to ≈ 150 . Under these conditions, it has a relatively short dead time and a large bandwidth. Therefore it is possible to use it for pulsed EPR experiments.

This work gives us confidence in the finite integration simulations. They can be used in the future to design and verify the properties of LGR and DR probes housed in cavities or microwave shields.

Acknowledgments

SMM thanks the Natural Sciences and Engineering Research Council of Canada for financial support in the form of discovery (operating) and equipment grants. SYN acknowledges financial

support from the University of New Brunswick in the form a predoctoral teaching assistantship. Valuable discussions with Professor R. Tervo are also acknowledged.

References

- [1] M. Bennati, T.F. Prisner, New developments in high field electron paramagnetic resonance with applications in structural biology, *Rep. Prog. Phys.* 68 (2005) 411–448.
- [2] J. Gendell, J.H. Freed, G.K. Fraenkel, Solvent effects in electron spin resonance (ESR) spectra, *J. Chem. Phys.* 37 (1962) 2832–2841.
- [3] D. Goldfarb, Electron paramagnetic resonance applications to catalytic and porous materials, *Electron Paramagn. Reson.* (2009) 451–487.
- [4] M.M. Hertel, V.P. Denysenkov, M. Bennati, T.F. Prisner, Pulsed 180-GHz EPR/ENDOR/PELDOR spectroscopy, *Magn. Reson. Chem.* 43 (2005) S248–S255.
- [5] J.S. Hyde, Trends in EPR technology, *Biol. Magn. Reson.* 24 (2005) 409–428.
- [6] G. Jeschke, Y. Polyhach, Distance measurements on spin-labeled biomacromolecules by pulsed electron paramagnetic resonance, *Phys. Chem. Chem. Phys.* 9 (2007) 1895–1910.
- [7] G.R. Eaton, S.S. Eaton, Electron–nuclear double resonance spectroscopy and electron spin echo envelope modulation spectroscopy, *Comp. Coord. Chem. II* 2 (2004) 49–55.
- [8] G. Feher, R.C. Fletcher, E.A. Gere, Exchange effects in spin resonance of impurity atoms in silicon, *Phys. Rev.* 100 (1955) 1784–1786.
- [9] B.M. Hoffman, Electron–nuclear double resonance spectroscopy (and electron spin–echo envelope modulation spectroscopy) in bioinorganic chemistry, *Proc. Natl. Acad. Sci. USA* 100 (2003) 3575–3578.
- [10] L.D. Kispert, Electron–electron double resonance, *Biol. Magn. Reson.* 24 (2005) 165–197.
- [11] Y.D. Tsvetkov, Peptide aggregation and conformation properties as studied by pulsed electron–electron double resonance: pulsed ELDOR in spin labeled peptides, *Biol. Magn. Reson.* 21 (2004) 385–433.
- [12] S.S. Eaton, G.R. Eaton, Measurements of interspin distances by EPR, *Electron Paramagn. Reson.* 19 (2004) 318–337.
- [13] J. McCracken, Electron spin echo envelope modulation (ESEEM) spectroscopy, *Appl. Phys. Methods Inorg. Bioinorg. Chem.* (2007) 55–77.
- [14] P.P. Borbat, J.H. Davis, S.E. Butcher, J.H. Freed, Measurement of large distances in biomolecules using double-quantum filtered refocused electron spin-echoes, *J. Am. Chem. Soc.* 126 (2004) 7746–7747.
- [15] Y.-W. Chiang, P.P. Borbat, J.H. Freed, The determination of pair distance distributions by pulsed ESR using Tikhonov regularization, *J. Magn. Reson.* 172 (2005) 279–295.
- [16] S.K. Misra, P.P. Borbat, J.H. Freed, Calculation of double-quantum-coherence two-dimensional spectra: distance measurements and orientational correlations, *Appl. Magn. Reson.* 36 (2009) 237–258.
- [17] J.E. Banham, C.M. Baker, S. Ceola, I.J. Day, G.H. Grant, E.J.J. Groenen, C.T. Rodgers, G. Jeschke, C.R. Timmel, Distance measurements in the borderline region of applicability of CW EPR and DEER: a model study on a homologous series of spin-labeled peptides (1969–1992), *J. Magn. Reson.* 191 (2008) 202–218.
- [18] C. Calle, A. Srekanth, M.V. Fedin, J. Forrer, I. Garcia-Rubio, I.A. Gromov, D. Hinderberger, B. Kasumaj, P. Leger, B. Mancosu, G. Mitrikas, M.G. Santangelo, S. Stoll, A. Schweiger, R. Tschaggelar, J. Harmer, Pulse EPR methods for studying chemical and biological samples containing transition metals, *Helv. Chim. Acta* 89 (2006) 2495–2521.
- [19] P.G. Fajer, Site directed spin labelling and pulsed dipolar electron paramagnetic resonance (double electron–electron resonance) of force activation in muscle, *J. Phys. Condens. Matter* 17 (2005) S1459–S1469.
- [20] T. Ikoma, Nanoscale rule. Electron–spin dipole–dipole interaction spectroscopy, *Kagaku to Kogyo (Tokyo, Jpn.)* 55 (2002) 576.
- [21] L. Millhauser Glenn, Copper and the prion protein: methods, structures, function, and disease, *Annu. Rev. Phys. Chem.* 58 (2007) 299–320.
- [22] T. Christides, W. Froncisz, T. Oles, J.S. Hyde, Probehead with interchangeable loop-gap resonators and RF coils for multifrequency EPR/ENDOR, *Rev. Sci. Instrum.* 65 (1994) 63–67.
- [23] R.W. Dykstra, G.D. Markham, A dielectric sample resonator design for enhanced sensitivity of EPR spectroscopy, *J. Magn. Reson.* 69 (1986) 350–355.
- [24] W. Froncisz, J.S. Hyde, The loop-gap resonator: a new microwave lumped circuit ESR sample structure, *J. Magn. Reson.* 47 (1982) 515–521.
- [25] W. Froncisz, T. Oles, J.S. Hyde, Q-band loop-gap resonator, *Rev. Sci. Instrum.* 57 (1986) 1095–1099.
- [26] J.P. Hornak, J.H. Freed, Electron spin echoes with a loop-gap resonator, *J. Magn. Reson.* 62 (1985) 311–313.
- [27] W.L. Hubbell, W. Froncisz, J.S. Hyde, Continuous and stopped flow EPR spectrometer based on a loop gap resonator, *Rev. Sci. Instrum.* 58 (1987) 1879–1886.
- [28] S. Pfenninger, J. Forrer, A. Schweiger, T. Weiland, Bridged loop–gap resonator: a resonant structure for pulsed ESR transparent to high-frequency radiation, *Rev. Sci. Instrum.* 59 (1988) 752–760.
- [29] F.J. Rosenbaum, Dielectric cavity resonator for ESR experiments, *Rev. Sci. Instrum.* 35 (1964) 1550–1554.
- [30] S.E. Bromberg, I.Y. Chan, Enhanced sensitivity for high-pressure EPR using dielectric resonators, *Rev. Sci. Instrum.* 63 (1992) 3670–3673.
- [31] S. Del Monaco, J. Brivati, G. Gualtieri, A. Sotgiu, Dielectric resonators in a TE₁₀₂ x-band rectangular cavity, *Rev. Sci. Instrum.* 66 (1995) 5104–5107.
- [32] M. Jaworski, A. Sienkiewicz, C.P. Scholes, Double-stacked dielectric resonator for sensitive EPR measurements (1969–1992), *J. Magn. Reson.* 124 (1997) 87–96.
- [33] A. Sienkiewicz, A.M.d.C. Ferreira, B. Danner, C.P. Scholes, Dielectric resonator-based flow and stopped-flow EPR with rapid field scanning: a methodology for increasing kinetic information, *J. Magn. Reson.* 136 (1999) 137–142.
- [34] A. Sienkiewicz, M. Jaworski, B.G. Smith, P.G. Fajer, C.P. Scholes, Dielectric resonator-based side-access probe for muscle fiber EPR study, *J. Magn. Reson.* 143 (2000) 144–152.
- [35] A. Sienkiewicz, K. Qu, Dielectric resonator-based stopped-flow electron paramagnetic resonance, *Rev. Sci. Instrum.* 65 (1994) 68–74.
- [36] K. Qu, J.L. Vaughn, A. Sienkiewicz, C.P. Scholes, J.S. Fetrow, Kinetics and motional dynamics of spin-labeled yeast iso-1-cytochrome c: 1. Stopped-flow electron paramagnetic resonance as a probe for protein folding/unfolding of the C-terminal helix spin-labeled at cysteine 102, *Biochemistry* 36 (1997) 2884–2897.
- [37] J.W.M. Walsh, J.L.W. Rupp, Enhanced ESR sensitivity using a dielectric resonator, *Rev. Sci. Instrum.* 57 (1986) 2278–2279.
- [38] I. Golovina, I. Geifman, A. Belous, New ceramic EPR resonators with high dielectric permittivity, *J. Magn. Reson.* 195 (2008) 52–59.
- [39] S.M. Mattar, A.H. Emwas, A tuneable doubly stacked dielectric resonator housed in an intact TE₁₀₂ cavity for electron paramagnetic resonance spectroscopy, *Chem. Phys. Lett.* 368 (2003) 724–731.
- [40] Y.E. Nesmelov, J.T. Surek, D.D. Thomas, Enhanced EPR sensitivity from a ferroelectric cavity insert, *J. Magn. Reson.* 153 (2001) 7–14.
- [41] A. Blank, E. Stavitski, H. Levanon, Transparent miniature dielectric resonator for electron paramagnetic resonance experiments, *Rev. Sci. Instrum.* 74 (2003) 2853–2859.
- [42] J.S. Hyde, in: M.C.R. Symons (Ed.), *Electron spin resonance*, The Royal Society of Chemistry, London, 1986, pp. 175–184.
- [43] J.S. Hyde, in: A.J. Hoff (Ed.), *Advanced EPR in biology and chemistry*, Elsevier, Amsterdam, 1989.
- [44] G.A. Rinard, R.W. Quine, S.S. Eaton, G.R. Eaton, Microwave coupling structures for spectroscopy, *J. Magn. Reson., Ser. A* 105 (1993) 137–144.
- [45] R.R. Mett, J.W. Sidabras, J.S. Hyde, Coupling of waveguide and resonator by inductive and capacitive irises for EPR spectroscopy, *Appl. Magn. Reson.* 35 (2008) 285–318.
- [46] W. Piasecki, W. Froncisz, J.S. Hyde, Bimodal loop-gap resonator, *Rev. Sci. Instrum.* 67 (1996) 1896–1904.
- [47] T. Oles, J.S. Hyde, W. Froncisz, Gordon coupler for K-band EPR loop gap resonator, *Rev. Sci. Instrum.* 60 (1989) 389–391.
- [48] G. Elger, J.T. Torring, K. Mobius, Novel loop-gap probe head for time-resolved electron paramagnetic resonance at 9.5 GHz, *Rev. Sci. Instrum.* 69 (1998) 3637–3641.
- [49] J.R. Anderson, R.A. Venters, M.K. Bowman, A.E. True, B.M. Hoffman, ESR and ENDOR applications of loop-gap resonators with distributed circuit coupling (1969), *J. Magn. Reson.* 65 (1985) 165–168.
- [50] R.D. Britt, M.P. Klein, A versatile loop-gap resonator probe for low-temperature electron spin-echo studies (1969), *J. Magn. Reson.* 74 (1987) 535–540.
- [51] C.S. Technology, Microwave studio 2010, Darmstadt, Germany, 2010.
- [52] M. Clemens, T. Weiland, Discrete electromagnetism with the finite integration technique, *Prog. Electromagn. Res.* 32 (2001) 65–87.
- [53] S. Fiedziuszko, A. Jalenski, Double dielectric resonator (correspondence), *Microwave Theory Tech, IEEE Trans* 19 (1971) 779–781.
- [54] R.R. Mett, J.W. Sidabras, I.S. Golovina, J.S. Hyde, Dielectric microwave resonators in TE₀₁₁ cavities for electron paramagnetic resonance spectroscopy, *Rev. Sci. Instrum.* 79 (2008) 094702–094708.
- [55] E.R. Davidson, The iterative calculation of a few of the lowest eigenvalues and corresponding eigenvectors of large real-symmetric matrices, *J. Comput. Phys.* 17 (1975) 87–94.
- [56] K. Gallivan, E. Grimme, P. VanDooren, A rational lanczos algorithm for model reduction, *Algorithms* 12 (1996) 33–63.
- [57] T. Itoh, R.S. Rudokas, New method for computing the resonant frequencies of dielectric resonators (short papers), *Microwave Theory Tech, IEEE Trans* 25 (1977) 52–54.
- [58] C.P. Poole, *Electron Spin Resonance*, second ed., A Comprehensive Treatise on Experimental Techniques, John Wiley and Sons, New York, 1983.
- [59] D.M. Pozar, *Microwave Engineering*, second ed., John Wiley and Sons, Hoboken, 2005.